J. Electrochem. Sci. Eng. **14(5)** (2024) 547-558; http://dx.doi.org/10.5599/jese.1955

Open Access : : ISSN 1847-9286
https://pub.iapchem.org/ojs/index.php/JESE

Original scientific paper

Optimizing power output in direct formic acid fuel cells using palladium film mediation: experimental and DFT studies

Christogonus O. Akalezi[1,2,✉], Arinze C. Maduabuchi[1,3], Simeon Nwanonenyi[1,4] and Emmanuel E. Oguzie[1]

[1]*Center of Excellence in Future Energies and Electrochemical Systems (ACEFUELS), Federal University of Technology, Owerri, Nigeria*
[2]*Department of Chemistry School of Physical Sciences, Federal University of Technology, Owerri, Nigeria*
[3]*Deparment of Science Laboratory Technology, Federal University of Technology, Owerri, Nigeria*
[4]*Department of Polymer and Polymer Technology, Federal University of Technology, Owerri, Nigeria*

Corresponding authors: ✉christogonus.akalezi@futo.edu.ng; *Tel.: 08080587128*

Received: June 26, 2023; Accepted: July 31, 2024; Published: August 25, 2024

Abstract

Low-temperature hydrogen production from environmentally friendly liquid fuels such as methanol, ethanol, and formic acid for miniature fuel cells used in powering portable electronic devices is attracting reasonable attention. In this study, we present the findings from the decomposition of formic acid and subsequent power generation within a microfluid fuel cell. The fuel cell system was engineered to incorporate a palladium membrane at the anode and a modified carbon Torray paper at the cathode. To assess fuel cell performance, we employed chronopotentiometry and cyclic voltammetric electro-chemical techniques. This simple fuel cell could achieve a current peak of 3.17 µW by utilizing 2.50 M HCOOH solution and 2.26 µW with 0.1 M solution, all at room temperature. Finally, to provide a deeper understanding of the reactivity and HCOOH decomposition pathways on various palladium surfaces, we conducted density functional theory (DFT) studies. Our DFT investigations revealed that the Pd(111) surface exhibited more negative adsorption energy compared to other surfaces, suggesting its propensity for a more isomeric crystal morphology. This research underscores the promising potential of low-temperature hydrogen production using safe liquid fuels in microfuel cell applications for portable electronic devices.

Keywords

Hydrogen production; formic acid decomposition; Pd catalyst; current peak; density functional theory

Introduction

Since the pioneering experiments of Benjamin Franklin in the 18th century and subsequent advancements by notable figures like Michael Faraday and Thomas Edison, electricity has progressively become an integral part of our daily lives. As a crucial energy carrier, electricity facilitates an array of essential services, including lighting, heating, refrigeration, and information technologies [1,2]. Despite its undeniable importance, electricity generation has long been associated with significant challenges, primarily from reliance on fossil fuels.

However, the conventional methods of generating electricity from fossil fuels have two major drawbacks. First is the alarming emission of CO_2, a primary driver of the greenhouse effect leading to severe climate change. These emissions trap heat within the atmosphere, prompting the need for sustainable energy solutions. Second, the finite nature of fossil fuel reserves underscores the necessity for alternative energy sources. To grapple with these challenges, the evolution of fuel cell technology has emerged as a promising avenue to harness energy with unparalleled efficiency and environmental resilience [2-5]. Notably, fuel cells possess a superior thermodynamic efficiency that holds the potential to mitigate greenhouse gas emissions.

Certain types of fuel cells, such as the proton-exchange membrane fuel cell (PEMFC), operate exclusively on pure hydrogen gas and oxygen, emitting only heat and water vapor into the environment [6,7]. Recent advancements in fuel cell technology-enabled direct utilization of reactive chemicals like methanol, ethanol, formic acid, and ammonia gas. These fuel cells, known as direct liquid fuel cells (DLFCs), utilize liquid fuels directly, oxidizing them at the anode without the need for reforming [8-10]. Its particular variant, a direct methanol fuel cell (DMFC), represents a notable example. However, DLFCs, including DMFCs, face unique challenges not encountered by their PEMFC counterparts.

The success of DLFCs relies on special materials, like gold, platinum, and palladium, which act as catalysts to facilitate chemical reactions [11-15]. The direct formic acid fuel cell (DFAFC) represents a promising advancement but faces unique challenges, such as slow reactions and fuel crossover [16,17]. Fuel crossover can lead to wasted energy and reduced efficiency. Additionally, DFAFC reactions can produce substances that hinder the effectiveness of catalyst [16-18].

To tackle these issues, our study combines experimental results with computer simulations to understand how formic acid breaks down and how the catalyst behaves. By exploring the speed and energy aspects of chemical reactions and their impact on catalysts, we aim to discover insights that can enhance energy conversion technology [16-20]. Also, computer simulations should help to see the details of how reactions happen [21-23]. This collaborative approach between experimental and virtual simulations should give a fresh perspective on how formic acid (FA) behaves on palladium catalysts. Our study brings a new angle in a field where virtual tools like the adsorption locator module are relatively unexplored.

This study should contribute to the field through its computational analyses of formic acid decomposition on palladium, utilizing the adsorption locator module. To the best of our knowledge, such a comprehensive computational exploration of this nature is lacking in the current body of research. By bridging theory and experiment, the paper aims to offer a robust foundation for evaluating electrode/electrolyte assemblies during formic acid decomposition, thus enriching our understanding of DLFCs and paving the way for advancements in sustainable energy technologies.

Experimental

Fuel cell configuration

Our study employed a 75 mL fuel cell obtained from the University of Bath, UK, containing the membrane-electrode assembly (MEA) at its centre. This innovative MEA utilizes a 0.025 mm thick palladium thin film (Goodfellows) that functions dually as both the proton conducting membrane and the catalyst. The film is precisely cut into a 5 mm square and then laminated, incorporating a central circular hole to expose the palladium to the solutions within the assembled cell. The cathode electrode, also 5 mm², is comprised of a carbon fiber composite base (Toray Paper 030) modified with a 3:1 (v/w) isopropanol solution containing Pt/C catalyst (Johnson Matthey). To facilitate efficient proton conduction during oxygen reduction, 1 µL of Nafion 117 solution (Aldrich Chemicals) was used to bind the catalyst particles. A copper tape ensured the electrical connection of both electrodes to the potentiostat. A 10 mM HCl solution was consistently used as the electrolyte. Figure 1 is the schematic of the fuel cell used for this study.

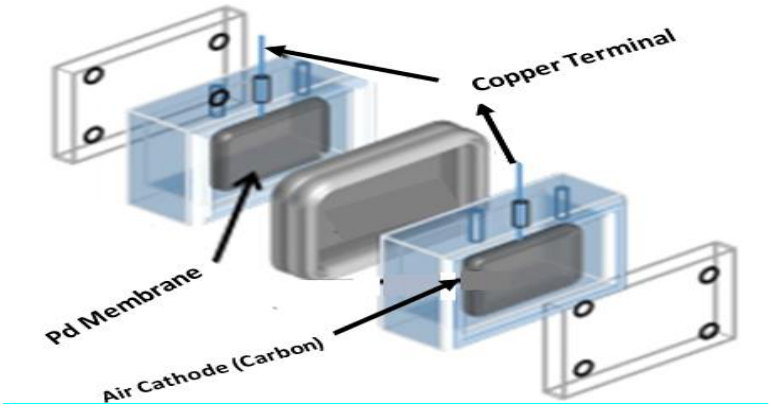

***Figure 1**. The fuel cell assembly*

Instrumentation

An Autolab potentiostat system (PGSTAT12, EcoChemie, Netherlands) was employed for the electrochemical experiments. Cyclic voltammetry (CV) and chronopotentiometry (CP) tests were used to test the electrode performance. In each solution, the CV experiments started at the open circuit potential (OCP), and the potential was scanned at a scan rate of 0.01 Vs^{-1} from 0.83 V negatively to 0.00 V and then in a positive direction toward OCP. Chronoamperometry data were obtained with the potential held at 0.1 V *vs.* SCE. The cell was allowed to equilibrate for 300-400 s before the fuel was added.

Metal plane simulations and computational methods

The density functional theory (DFT) study was conducted using Adsorption Locator Tools, available in BIOVIA Materials Studio (MS 7.0).

The aim was to understand the activities of the available Pd (111), (110), and (100) crystal planes for the electrochemical reduction of formic acid against bulk crystal [24]. During the calculations, a (3×4) supercell mesh was used, built upon 1.5-layer Pd slabs with a 100 nm vacuum gap [25,26]. Only the surface atoms were fixed to eliminate the interactions between slabs, while other layers and the adsorbed species were relaxed. The geometry and energy of Pd metal planes and molecules were optimized using the generalized gradient corrected approximation (GGA) method available in the Forcite tool module [26], a Perdew-Burke-Ernzerhof (PBE) function with a DNP basis set to account for exchange-correlation effects. We also applied the COMPASS (Condensed-phase

optimized molecular potentials for atomistic simulation studies) during the optimization process. The COMPASS force field can simulate the gas and condensed-phase properties of materials with high accuracy [27]. The adsorption locator tool was used to determine the possible low-energy adsorption sites of the optimized molecules on the metal surfaces/planes. The adsorption processes were studied on all three three crystal planes (Pd (100, 110, 111)) to determine the sites with the most affinity towards the adsorption of the FA decomposition products.

Results and discussion

Figure 2 illustrates the relationship between formic acid concentration and hydrogen generation/ /diffusion through a palladium membrane using zero current chronopotentiometry. Before fuel introduction, the potential stabilizes around 0.45 V. This indicates a settling period for the system to reach equilibrium before initiating the reaction. Introducing 0.1 M formic acid triggers a current increase. This corresponds to the oxidation of newly generated hydrogen molecules that have permeated the palladium membrane after formic acid catalysis.

Compared to 0.1 M, a significantly larger and faster change occurs upon adding 2.5 M formic acid. This signifies a more rapid rate of hydrogen generation and diffusion through the membrane.

The data presented in Figure 2 demonstrates a direct correlation between formic acid concentration and the efficiency of hydrogen production and permeation through the palladium membrane. Higher formic acid concentrations lead to faster reaction rates and increased hydrogen flux.

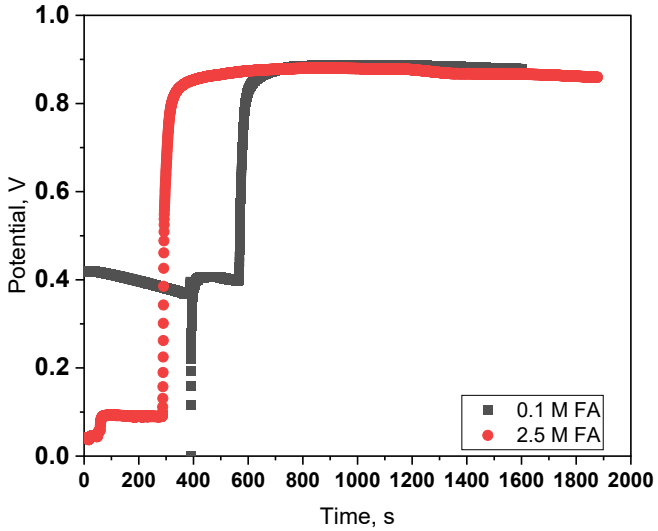

Figure 2. *Zero current chronopotentiometry in 10 mM HCl in contact with a palladium membrane. Aqueous solution of either 0.1 M or 2.5 M formic acid is injected into the fuel compartment to trigger hydrogen generation and hydrogen permeation through palladium*

Figure 3 represents the CVs recorded for the formic acid decomposition (FAD) on a Pd electrode at 0.1 M and 2.5 M formic acid in 10 mM HCl solutions at 30 °C.

Several studies on FAD [28-31] reported that carbon monoxide (CO) (a major poisoning intermediate species) oxidation reaction on pure metals commenced between E = 0.4 to 0.6 V at ambient temperature. In this regard, the species giving the signal at E = 0.6 V (Figure 3) must be hydrogen gas, which evolved at the Pd membrane. Beyond CO, other intermediate species have been proposed in the decomposition of formic acid (HCOOH). Hu *et al.* [32] postulated formate (HCOO*) as the primary intermediate, while Zhang *et al.* [33-35] suggested a mechanism involving both formate (HCOO*) and carboxyl (*COOH) radicals. These intermediates are implicated in the following reactions, Eqs. (1)-(4):

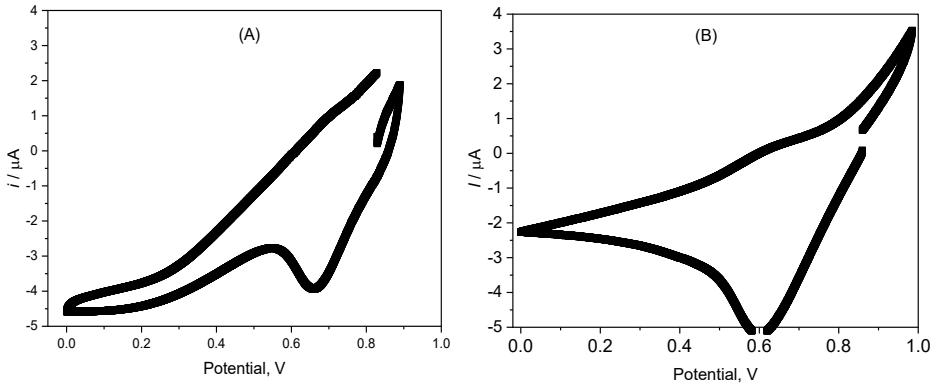

Figure 3. *Cyclic voltammogram for a smooth Pd electrode at 30 °C in 10 mM HCl and (A) 0.1 M and (B) 2.5 M HCOOH (from the open circuit (0.83 V) scanning towards 0.0 V), scan rate 10 mV s^{-1} showing indirect fuel cell power generation*

$$HCOOH^* + \rightarrow HCOO^* + H^* \quad (1)$$

$$HCOOH^* + \rightarrow {}^*COOH + H^* \quad (2)$$

$$HCOO^* + \rightarrow CO_2^* + H^* \quad (3)$$

$$^*COOH + \rightarrow CO_2^* + H^* \quad (4)$$

Barbir [36] proposed an auto-inhibitory mechanism for formic acid oxidation on palladium, involving the following steps, Eqs. (5)-(7):

$$Pd + HCOOH \rightarrow Pd(HCOO)_{ad} + H^+ + e^- \quad (5)$$

$$Pd + HCOOH + Pd(HCOO)_{ad} \rightarrow Pd_2(C(OH)_2)_{ad} + CO_2 + H^+ + e^- \quad (6)$$

$$Pd_2(C(OH)_2)_{ad} \rightarrow 2Pd + CO_2 + 2e^- \quad (7)$$

According to Barbir's model [36], the formation of $Pd(HCOO)_{ad}$ (Eq. (5)) is followed by the formation of $Pd_2(C(OH)_2)$ad (Eq. (6)), which eventually decomposes to regenerate the palladium catalyst and produce CO_2 (Eq. (7)). The accumulation of $Pd_2(C(OH)_2)_{ad}$ is suggested to inhibit the overall reaction rate.

Figure 4 illustrates the cyclic voltammograms of the fuel cell using 0.1 M and 2.50 M formic acid solutions, generating power outputs of 2.26 and 3.17 µW, respectively. Concentration overpotential is the primary factor contributing to this observed difference in power output. At higher formic acid concentrations, there might be a decrease in the concentration overpotential due to the higher availability of reactants at the electrode surface. This can lead to a more favorable voltage behavior in the DFAFC operating with 2.5 M formic acid compared to 0.1 M.

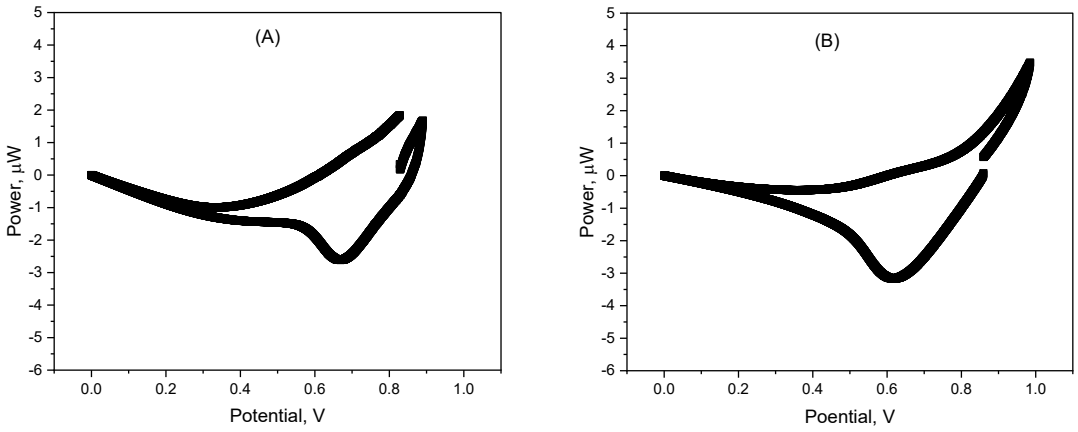

Figure 4. *Voltammetry data (scan rate 10 mV/s) showing indirect fuel cell power generation obtained from the system containing (a) 10 mM HCl + 0.1M and (B) 10 mM HCl + 2.5 M HCOOH*

The oxidation of formic acid at the anode is a complex electrochemical reaction involving several intermediate steps, and higher concentrations could potentially enhance the reaction rate, leading to a higher current density and a more favorable voltage response in the DFAFC with 2.5 M formic acid.

The transport of reactants and products within the fuel cell, including ions, can also play a significant role in determining the overall performance. A higher concentration of formic acid might lead to better mass transport of reactants to the electrode surface, resulting in improved overall cell performance.

Adsorption locator simulations

Monte Carlo simulation can make understanding the reactions of adsorbed species, desorption, dissociation, and or diffusion possible. Before this investigation, two issues were taken into consideration. FA decomposition on pure metal catalysts is usually explained as a dual-path mechanism [37-39], which was originally proposed by Capon *et al*. [40](Eq.8):

$$\mathrm{HCOOH} \begin{cases} \text{Reaction intermediate} \longrightarrow \mathrm{CO_2 + 2H^+ + 2e^-} \\ \mathrm{CO_{ad} + OH_{ad} + H^+ + e \longrightarrow CO_2 + 2H^+ + 2e^-} \end{cases} \quad (8) \qquad (8)$$

The indirect pathway leads to CO formation, followed by its electrooxidation to CO_2, while the direct pathway involves the direct formation of CO_2 (without producing CO). The path leading to CO formation represents a major problem for Pd-based fuel cells since the adsorbed CO acts as a poison, limiting the fuel cell operation.

The other issue concerns water in the physical system, not just as a decomposition product but also as a significant participant in the electrochemical redox process. Based on this dual pathway decomposition of formic acid, we created four systems (A-D) containing four different adsorbates: FA/H_2/CO_2, FA/H_2/CO_2/H_2O, FA/CO/H_2O, and FA/H_2/CO/CO_2/H_2O. We studied the adsorption of the FA molecule as a mixture with the other decomposition products to determine the effect of each species on the adsorption energies. We assumed that no member of the decomposition product could act in isolation within the cell. The systems were studied initially on the basis of equal mole ratio loading but later with increasing hydrogen loading in the fourth system (system D). Since the electrochemical and mechanistic analysis confirmed the generation of CO, and hydrogen within the system, it suggests that the two decomposition pathways were occurring simultaneously, and this is only possible in system D. This observation agrees with the view expressed by He *et al*. [21] that both dehydration and dehydrogenation reactions will be unselective in the aqueous phase due to very small difference in the enthalpies of formation of CO and CO_2.

The energy changes obtained for the adsorbate species over Pd(100), Pd(110), and Pd(111) surfaces for systems (A-D) are displayed in Table 1. The total energy column represents the sum of the adsorption energies and the internal energies of the adsorbed species. Adsorption energy is a key energy parameter for adsorption and represents the energy needed for the adsorption of a relaxed adsorbate on the metal substrate. The adsorption energy is the sum of both the deformation and rigid adsorption energies. The rigid adsorption energy is the energy released when an unrelaxed molecule is adsorbed on the metal surface. Deformation indicates the energy released by adsorbed species relaxing on the substrate after adsorption. The dE_{ad}/dn, is a change in adsorption energy with respect to a change in the number of adsorbed molecules (FA, H_2, CO_2, H_2O or CO). It quantifies the change in energy associated with adding or removing a single molecule from the substrate [25-28]. A higher absolute value of dE_{ad}/dn indicates a stronger interaction between the molecule and the substrate, making desorption more difficult. Low values of desorption energy for H_2 obtained over the three Pd

planes demonstrate less stable adsorption of H_2. The value of desorption energy of the individual molecules follows the trend: FA > CO_2 > H_2O > CO. The energy values reported in this simulation were the average of 10 configurations. As indicated in Table 1, systems with only individual adsorbates showed positive total energy for adsorption, indicating relatively low adsorption, which confirms that condensed-phase adsorption is favourable on Pd metal surfaces [21]. We observed that the adsorption energy calculated by the adsorption locator for the Pd(111) face is more negative than the other faces; hence Pd(111) was adopted as a more isometric crystal morphology.

Table 1*. Parameters for different adsorbate-metal substrate configurations on three crystalline planes obtained for FA/H_2/CO_2, FA/H_2/CO_2/H_2O, FA/CO/H_2O, and FA/H_2/CO/CO_2/H_2O systems through adsorption locator simulations*

System	Energy, J / mol				(dE_{ad} / dn) / (J / mol)				
	Total	Adsorption	Rigid adsorption	Deformation	FA	H_2	CO_2	H_2O	CO
Substrate	0.0000								
FA:	51.8339								
H_2	6.0136×10^{-4}								
CO	216.4083								
CO_2	216.3936								
H_2O	77.2288								
FA/H_2/CO_2 @Pd(100)	234.1778	-38.5818	-38.5817	2.3774×10^{-9}	-26.2900	-0.9243	-20.1292		
FA/H_2/CO_2 @Pd(110)	234.8962	-35.4873	-35.4873	2.1629×10^{-9}	-23.9258	-0.9632	-19.1983		
FA/H_2/CO_2 @Pd(111)	-59.8143	-332.1939	-38.3719	-293.8220	-103.3635	-0.8548	-234.6601		
FA/H_2/CO_2/H_2O@Pd(100)	294.3301	-55.7169	-55.7169	1.5211×10^{-9}	-32.0693	-0.8787	-19.1136	-20.5688	
FA/H_2/CO_2/H_2O@Pd(110)	294.4412	-52.8181	-52.8181	6.0383×10^{-9}	-32.4553	-0.5322	-18.3766	-18.3709	
FA/H_2/CO_2/H_2O@Pd(111)	-32.8321	-380.9517	-51.3676	-329.5840	-104.5479	-0.8812	-229.3645	-53.7568	
FA/CO/H_2O @Pd(100)	200.7333	-46.9365	-46.9365	8.98670×10^{-10}	-28.4411			-21.4924	-7.8763
FA/CO/H_2O @Pd(110)	200.0372	-46.0654	-46.0654	3.2979×10^{-9}	-28.5253			-21.1244	-8.5802
FA/CO/H_2O @Pd(111)	-26.7546	-272.5069	-45.0320	-227.4749	-102.7201			-52.4919	-123.2374
FA/H_2/CO/H_2O/CO_2@ Pd (100)	395.7815	-68.2812	-68.2812	-3.9447×10^{-9}	-34.5881	-0.8389	-21.4245	-21.4595	-9.1864
FA/H_2/CO/H_2O/CO_2@ Pd (110)	400.3920	-60.8830	-60.8830	3.7663×10^{-9}	-31.6886	-0.7617	-19.5056	-18.7893	-7.8366
FA/H_2/CO/H_2O/CO_2@ Pd (111)	-81.6005	-60.0427	-60.4523	0.4096	-31.2947	-0.85049	-17.3117	-17.7563	-9.3939

Figure 5 represents the field value output of the various systems obtained from the simulation. The regions of adsorption on different adsorbates on the Pd(111) lattice plane are depicted. The green spot regions over each plane indicate a favourable region for adsorption, while the red spot indicates improbable regions for adsorption.

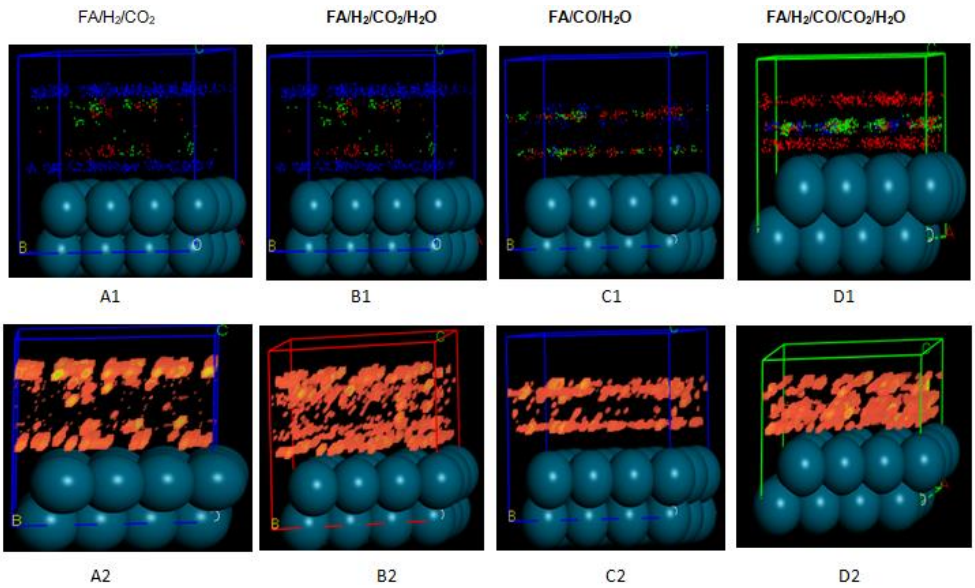

Figure 5. *Various regions of adsorption on the Pd (111) plane for four different systems are presented in normal view and colour-by-field values (lateral views only). Green spots are the most probable and red spots are the least probable regions for adsorption*

Figure 6 displays the optimized structures of different molecules (FA, H_2, CO_2, CO, and H_2O) and their adsorption configurations in a fully loaded cell.

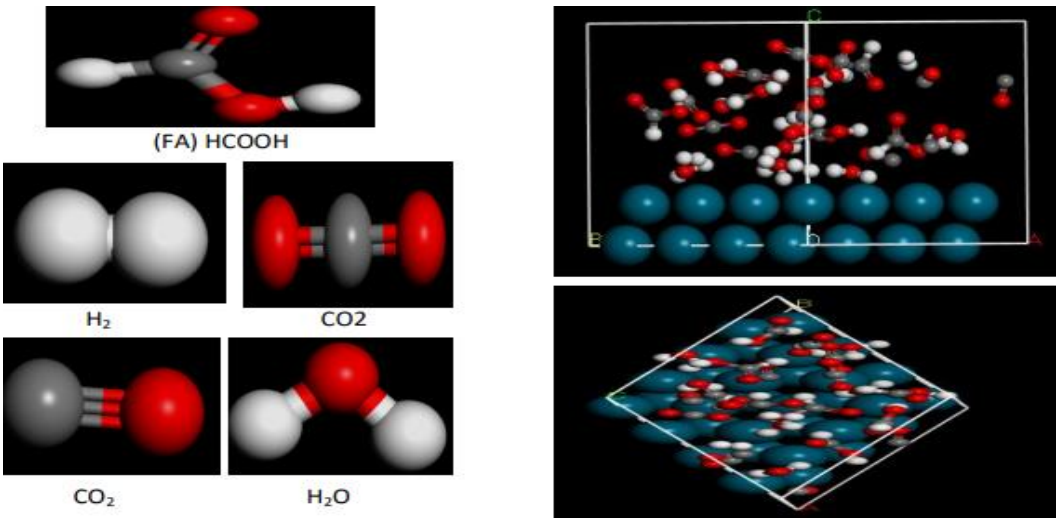

Figure 6. *Optimized structures of FA and its decomposition products. On the right is an amorphous cell output containing 6 of each molecule over the Pd(111) surface (side and top views). All available adsorption sites are equally portable*

Figure 7 represents the effect of increasing the hydrogen loading in the system, showing a lowering in the energy of the system with increasing hydrogen concentration.

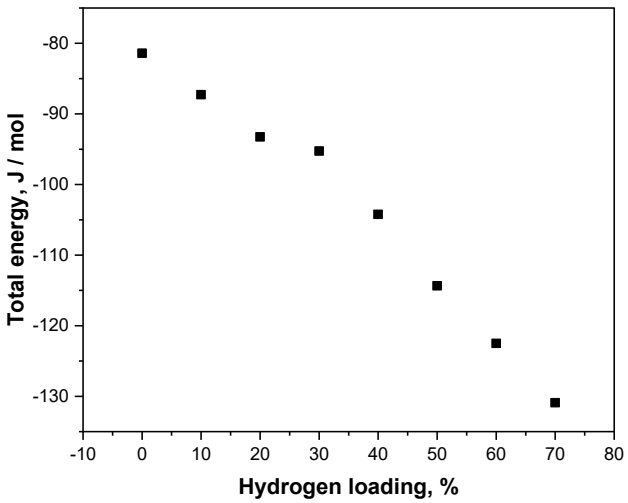

Figure 7*. Effect of increasing the hydrogen loading on the energy of the systems*

Binding energy assessment

The binding energy of the adsorbate species (E_{BE}) was calculated on the average of 10 configurations obtained for the planes Pd (111), Pd (110), and Pd (100). Here, the E_{BE} was calculated using equation (8) [41]:

$$E_{BE} = E_{Pd(jkl)}(FA/H_2/CO/CO_2/H_2O) - E_{Pd(jkl)} - E_{FA} - E_{H_2} - E_{CO} - E_{CO_2} - E_{H_2O} \quad (9)$$

where $E_{Pd(jkl)}(FA/H_2/CO/CO_2/H_2O)$ is the total energy of the configuration, $E_{Pd(jkl)}$ is the energy of the crystal plane, and E_{FA}, E_{H_2}, E_{CO}, E_{CO_2} and E_{H_2O} are energies of each isolated molecule, FA, H_2, H_2O, CO and CO_2

The values of E_{BE} calculated for the three planes and four systems are presented in Table 2. According to the equation (8), the values obtained for each plane demonstrated that the process of adsorption on each plane in the $FA/H_2/CO/CO_2/H_2O$ system was chemisorption [24,41].

***Table 2**. Binding energy for four systems calculated for Pd (100), Pd (110) and Pd (111) planes*

System	E_{BE} / kJ mol^{-1}		
	Pd(100)	Pd(110)	Pd(111)
FA/H_2/CO_2	-38.6672	-35.6523	-39.6368
FA/H_2/CO_2/H_2O	-56.0212	-52.4849	-54.7252
FA/CO/ H_2O	-47.2780	-45.1263	-46.2038
FA/H_2/CO/CO_2/H_2O	-59.7825	-64.0767	-59.5529

Conclusion

The search for sustainable future green energy resource solutions is in high gear and formic acid is one such resource. This study used a microfluid fuel cell to systematically follow a Pd-catalyzed formic acid decomposition reaction involving electrochemical and quantum chemical approaches. During the initial stage of the reaction, a constant signal can be observed from the chronopotentiogram, indicating the discharge of hydrogen ions on active sites. This reaction was suddenly stalled by a deactivation process, thus yielding a plot as a function of time. The adsorption energy calculation shows that the absorbable species include FA, CO_2, and H_2O, in addition to the well-known CO. These adsorbates tend to clog the catalyst active sites, thus reducing the efficiency of the system. However, they can be more efficient if the reaction is conditioned to yield more hydrogen than other decomposition products. The Monte Carlo simulation shed some light on the reactions' fundamentals, which is vital in optimizing the system.

***Conflicts of interest:** The authors declare no competing financial interest.*

***Acknowledgement:** The authors wish to gratefully acknowledge research support from TETFUND for Institutional based research (IBR-2020/2021).*

References

[1] N.Z. Muradov, T.N. Veziroğlu, "Green" path from fossil-based to hydrogen economy: An overview of carbon-neutral technologies, *International Journal of Hydrogen Energy* **33(23)** (2008) 6804-6839. https://doi.org/10.1016/j.ijhydene.2008.08.054

[2] S. A. Boudghene, E. Traversa, Fuel cells, an alternative to standard sources of energy, *Renewable and Sustainable Energy Reviews* **6** (2002) 295-304. https://doi.org/10.1016/S1364-0321(01)00015-6

[3] A. Dewan, S. U. Ay, M. N. Karim, H. Beyenal, Alternative power sources for remote sensors: A review, *Journal of Power Sources* **245** (2014) 129-143. https://doi.org/10.1016/j.jpowsour.2013.06.081

[4] S. Mekhilef, R. Saidur, A. Safari, Comparative study of different fuel cell technologies. *Renewable and Sustainable Energy Reviews* **16** (2012) 981-989. https://doi.org/10.1016/j.rser.2011.09.020

[5] J. Eppinger, K. -W. Huang, Formic Acid as a Hydrogen Energy Carrier, *ACS Energy Letters* **2** (2017) 188−195. https://doi.org/10.1021/acsenergylett.6b00574

[6] *Fuel Cell Handbook*, EG & G Technical Services, U.S. Department of Energy, Morgantown, West Virginia, 2004. https://www.netl.doe.gov/sites/default/files/netl-file/FCHandbook7.pdf

[7] G. Pandey, Biomass-based bio-electro fuel cells based on carbon electrodes: an alternative source of renewable energy, *SN Applied Sciences* **1** (2019) 408. https://doi.org/10.1007/s42452-019-0409-4

[8] S. Uhm, H. J. Lee, J. Lee, Understanding underlying processes in formic acid fuel cells, *Physical Chemistry Chemical Physics* **11** (2009) 9326-9336. https://doi.org/10.1039/B909525J

[9] N. R. Joshi, Development in Direct Methanol - Oxygen Fuel Cell (DMFC), *IOSR Journal of Applied Chemistry (IOSR-JAC)* **7(9)** (2014) 24-26. https://doi.org/10.9790/5736-07922426
[10] P. Joghee, J. N. Malik, S. Pylypenko, R. O'Hayre, A review on direct methanol fuel cells-In the perspective of energy and sustainability, *MRS Energy & Sustainability* ***2*** *(*2015). https://doi.org/10.1557/mre.2015.4
[11] K. Müller, K. Brooks, T. Autrey, Hydrogen Storage in Formic Acid: A Comparison of Process Options, *Energy & Fuels* **31** (2017) 12603-12611. https://doi.org/10.1021/acs.energyfuels.7b02997
[12] S. Fukuzumi, Production of Liquid Solar Fuels and Their Use in Fuel Cells, *Joule* **1** (2017) 689-738. https://doi.org/10.1016/j.joule.2017.07.007
[13] F. Sanchez, D. Motta, A. Roldan, C. Hammond, A. Villa, N. Dimitratos, Hydrogen Generation from Additive-Free Formic Acid Decomposition Under Mild Conditions by Pd/C: Experimental and DFT Studies,*Topics in Catalysis* **61** (2018) 254-266. https://doi.org/10.1007/s11244-018-0894-5
[14] D. Mellmann, P. Sponholz, H. Junge, M. Beller, Formic acid as a hydrogen storage material-development of homogeneous catalysts for selective hydrogen release, *Chemical Society Reviews* **45** (2016) 3954-3988. https://doi.org/10.1039/C5CS00618J
[15] S. Fukuzumi, T. Suenobu, Hydrogen storage, and evolution catalyzed by metal hydride complexes, *Dalton Transactions* **42** (2013) 18-28. https://doi.org/10.1039/C2DT31823G
[16] E. Madrid, C. Harabajiu, R.S. Hill, K. Black, L. Torrente-Murciano, A. J. Dickinson, P. J. Fletcher, K. I. Ozoemena, A. K. Ipadeola, E. Oguzie, C. O. Akalezi, F. Marken, Indirect Formic Acid Fuel Cell Based on a Palladium or Palladium-Alloy Film Separating the Fuel Reaction and Electricity Generation, *ChemElectroChem* **8** (2021) 378-385. https://doi.org/10.1002/celc.202001570
[17] A. K. Singh, S. Singh, A. Kumar, Hydrogen energy future with formic acid: a renewable chemical hydrogen storage system, *Catalysis Science & Technology* 6 (2016) 12-40. https://doi.org/10.1039/C5CY01276G
[18] B.Seger, G. Q. Lu, L. Wang, Electrical power and hydrogen production from a photo-fuel cell using formic acid and other single-carbon organics, *Journal of Materials Chemistry* **22** (2012) 10709-10715. https://doi.org/10.1039/C2JM16635F
[19] W. Güther, W. Vielstich, Investigation on the Electrocatalytic Dehydrogenation of CHO-Compounds in acidic media *via* a palladium membrane, *Electrochimica Acta* **27(7)** (1982) 811-816. https://doi.org/10.1016/0013-4686(82)80201-6
[20] S.-W. Ting, C. Hu, J.K. Pulleri, K-Y. Chan, Heterogeneous Catalytic Generation of Hydrogen from Formic Acid under Pressurized Aqueous Conditions, *Industrial & Engineering Chemistry Research* **51** (2012) 4861−4867. https://doi.org/10.1021/ie2030079
[21] N. He, Z. H. Li, Palladium-atom catalyzed formic acid decomposition and the switch of reaction mechanism with temperature, *Physical Chemistry Chemical Physics* **18** (2016) 10005-10017. https://doi.org/10.1039/C6CP00186F
[22] M. Rafiee, H. Bashiri, Dynamic Monte Carlo simulations of the reaction mechanism of hydrogen production from formic acid on Ni (100), *Applied Surface Science* **475** (2019) 720-728. https://doi.org/10.1016/j.apsusc.2018.12.294
[23] R. Zhang, M. Yang, M. Peng, L. Ling, B. Wang, Understanding the role of Pd:Cu ratio, surface and electronic structures in Pd-Cu alloy material applied in direct formic acid fuel cells, *Applied Surface Science* **465** (2019) 730-739. https://doi.org/10.1016/j.apsusc.2018.09.196
[24] A. Plauck, E. E. Stangland, J. A. Dumesic, M. Mavrikakis, Active Sites and Mechanisms for H_2O_2 Decomposition over Pd Catalysts, *Proceedings of the National Academy of Sciences (PNAS)* **113(14)** (2016) E1973-E1982. http://www.pnas.org/cgi/doi/10.1073/pnas.1602172113

[25] M. Rezakazemi, T. A. Kurniawan, A. B. Albadarin, S. Shirazian, Molecular Modeling Investigation on Mechanism of Phenol Removal from Aqueous Media by Single- and Multi-Walled Carbon Nanotubes, *Journal of Molecular Liquids* **271** (2018) 24-30. https://doi.org/10.1016/j.molliq.2018.08.132

[26] M. J. Harrison, D. P. Woodruff, J. Robinson, Density Functional Theory Investigation of the Structure of SO_2 and SO_3 on Cu(111) and Ni(111), *Surface Science* **600(9)** (2006) 1827-1836. https://doi.org/10.1016/j.susc.2006.02.020

[27] H. Sun, The COMPASS Force Field: Parameterization and Validation for Phosphazenes, *Computational and Theoretical Polymer Science* **8(1-2)** (1998) 229-246. https://doi.org/10.1016/S1089-3156(98)00042-7

[28] R. Zhang, H. Liu, B. Wang, L. Ling, Insights into the preference of CO_2 formation from HCOOH decomposition on Pd surface: A theoretical study, *The Journal of Physical Chemistry C* **116** (2012) 22266-22280. https://doi.org/10.1021/jp211900z

[29] Y. Zhu, Z. Khan, R. I. Masel, The behavior of palladium catalysts in direct formic acid fuel cells, *Journal of Power Sources* **139** (2005) 15-20. https://doi.org/10.1016/j.jpowsour.2004.06.054

[30] C. Rice, S. Ha, R. Masel, A.I. Wieckowski, Catalysts for direct formic acid fuel cells, *Journal of Power Sources* **115** (2003) 229-235. https://doi.org/10.1016/S0378-7753(03)00026-0

[31] Y. X. Chen, M. Heinen, Z. Jusys, R. J. Behm, Kinetics and mechanism of the electrooxidation of formic acid - Spectroelectrochemical studies in a flow cell, *Angewandte Chemie-International Edition* **45** (2006) 981-985. https://doi.org/10.1002/anie.200502172

[32] C. Hu, S.-W. Ting, K.-Y. Chang, W. Huang Reaction pathways derived from DFT for understanding catalytic decomposition of formic acid into hydrogen on noble metals, *International Journal of Hydrogen Energy* **37(10)** (2012) 15956-15865. https://doi.org/10.1016/j.ijhydene.2012.08.035

[33] Y. Wang, Y. Qi, D. Zhang, New mechanism of the direct pathway for formic acid oxidation on Pd(111), *Computational and Theoretical Chemistry* **1049** (2014) 51-54. https://doi.org/10.1016/j.comptc.2014.09.020

[34] J. S. Yoo, F. Abild-Pedersen, J. K. Nørskov, F. Studt, Theoretical analysis of transition-metal catalysts for formic acid decomposition, *ACS Catalysis* **4** (2014) 1226-1233. https://doi.org/10.1021/cs400664z

[35] Y. X. Chen, M. Heinen, Z. Jusys, R. J. Behm, Kinetic isotope effects in complex reaction networks: Formic acid electro-oxidation, *ChemPhysChem* **8** (2007) 380-385. https://doi.org/10.1002/cphc.200600520

[36] F. Barbir, *Fuel Cells - Exploratory Fuel Cells | Regenerative Fuel Cells*, in *Encyclopedia of Electrochemical Power Sources,* Jürgen Garche, Ed., Elsevier B.V. (2009), 224-237. https://doi.org/10.1016/b978-044452745-5.00288-4

[37] K. H. Kim, J.K. JYu, HS. Lee JH. Choi, SY. Noh, S.K. Yoon, C. S. Lee, T.S. Hwang, YW. Rhee, Preparation of Pt-Pd catalysts for direct formic acid fuel cell and their characteristics, *Korean Journal of Chemical Engineering* **24** (2007) 518-521. https://doi.org/10.1007/s11814-007-0091-x

[38] K. Jiang, H-X. Zhang, S. Zou, W-H. Cai, Electrocatalysis of formic acid on palladium and platinum surfaces: from fundamental mechanisms to fuel cell applications, *Physical Chemistry Chemical Physics* **16** (2014) 20360-20376. https://doi.org/10.1039/C4CP03151B

[39] X. Yang, P. Pachfule, Y. Chen, N. Tsumori, Q. Xu, Highly efficient hydrogen generation from formic acid using a reduced graphene oxide-supported AuPd nanoparticle catalyst, *Chemical Communications* **52(22)** (2016) 4171–4174. https://doi.org/10.1039/C5CC10311H

[40] A. Capon, R. Parsons. Oxidation of Formic-Acid at Noble-Metal Electrodes Part .3. Intermediates and Mechanism on Platinum-Electrodes, *Journal of Electroanalytical and Interfacial Chemistry* **45** (1973) 205-231. https://doi.org/10.1016/S0022-0728(73)80158-5

[41] X. Zhang, Z. Dai, Q. Chen, J. A. Tang, DFT study of SO_2 and H_2S gas adsorption on Au-doped single-walled carbon nanotubes, *Physica Scripta* **89(6)** (2014) 065803. https://doi.org/10.1088/0031-8949/89/6/065803